On Necessary Pumping Pressures for Industrial Process-Driven Particle-Laden Fluid Flows

T. I. Zohdi
Department of Mechanical Engineering,
University of California,
Berkeley, CA 94720-1740

Due to increasing demands for faster and faster manufacturing of new complex materials, such as casting of particulate composites, the determination of pumping pressures needed for particle-laden fluids through channels is critical. In particular, the increase in viscosity as a function of the particle volume fraction can lead to system malfunction, due to an inability to deliver necessary pressures to pump the more viscous fluid through the system. This paper studies the pressure gradient needed to maintain a given flow rate, explicitly as a function of the volume fraction of particles present in the fluid. It is also crucial to control voids in the casted products, which can be traced to air-entrainment, spurious internal reactions, dewetting, etc., which can be traced to high Reynolds numbers. Accordingly, an expression for the resulting Reynolds number as a function of the particle volume fraction and flow rate is also developed. Numerical examples are provided to illustrate the practical use of the derived relations to characterize the necessary pumping pressures for process-driven, particle-laden fluid flows.
[DOI: 10.1115/1.4030620]

1 Introduction

In a variety of industries, ranging from next generation engines, turbomachinery, printed electronics, food processing, etc., new types of heterogeneous materials, comprising particulates in a binding matrix, are being developed and utilized. The macroscopic material characteristics of the material are dictated by the aggregate response of an assemblage of particles suspended in a binding matrix material. In the fabrication of such materials, the basic philosophy is to select material combinations to produce desired aggregate responses. For example, in structural engineering applications, the classical choice is a harder particulate phase that serves as a stiffening agent for a ductile, easy to form, base matrix material. Oftentimes, such materials start in particulate form and are then mixed with a binder and delivered as a flowing slurry to be cast into their final shape.[1] Thus, because of the increasing demands for faster and faster manufacturing of new complex particle-laden materials, the determination of pumping pressures needed to move such fluids through channels is critical (Fig. 1).

For particle-laden fluids delivered through channels, the increase in viscosity can lead to system malfunction, due to an inability to supply necessary pressures to pump the more viscous material properly. This paper studies the pressure gradient needed to maintain a given flow rate, explicitly as a function of the volume fraction of particles present in the fluid. The expression is general and easy to apply for the analysis of pumping particle-laden fluids. Furthermore, it is crucial to control voids in the resulting casted products, which are correlated to air-entrainment, spurious internal reactions, dewetting, etc. These effects are correlated to high Reynolds numbers. Accordingly, an expression for the resulting Reynolds number as a function of the particle volume fraction and flow rate is also developed. Numerical examples are provided to illustrate the practical use of the derived relations to characterize the necessary pumping pressures for process-driven particle-laden fluid flows. Because, resulting voids may be impossible to avoid, we also determine their effects on the overall effective properties of a heterogeneous two-phase slurry consisting of particles and a binding interstitial material. Estimates are developed for the reduction of the overall mechanical and thermal properties, based on embedded, double application of the Hashin–Shtrikman bounds, whereby, on the first level, the effective properties due to voids are computed, and on the second level the smaller scale heterogeneous material is taken into account.[2] This research is also quite relevant to the development of high-resolution electrohydrodynamic-jet printing processes. For overviews, see Wei and Dong [1], where they also developed specialized processes employing phase-change inks. Such processes are capable of producing micron-level footprints for high-resolution additive manufacturing.

Remark. The objective of the analysis is to develop semi-analytical expressions that can help guide analysts who are designing manufacturing systems involving particle-laden flows. Clearly, one could approach the problem with a large-scale Computational Fluid Dynamics (CFD) analysis. However, for direct numerical simulation of particle-laden continua, spatiotemporal discretization grids must be extremely fine, with several thousand numerical unknowns needed per particle length-scale for numerically accurate results. Thus, for several hundred thousand particles in a system, a proper discretization would require several billion numerical unknowns (see, for example, Onate et al. [2,3], Rojek et al. [4], Carbonell et al. [5], Labra and Onate [6], Leonardi et al. [7], Cante et al. [8], Rojek [9], Onate et al. [10], Bolintineanu et al. [11], Avci and Wriggers [12], and Zohdi [13,14], and Zohdi and Wriggers [15]. Although such simulations are possible in high-performance computing centers, their usefulness for rapid daily design analysis is minimal. This will be discussed further in the summary.

2 Channel Flow

As indicated in Sec. 1, the presence of secondary particles in fluids, particularly within channels, is wide-ranging and their

[1]Over 50% (by mass) of man-made materials start in granulated form.

Contributed by the Manufacturing Engineering Division of ASME for publication in the Journal of Manufacturing Science and Engineering. Manuscript received March 28, 2015; final manuscript received May 8, 2015; published online October 1, 2015. Assoc. Editor: Donggang Yao.

[2]Generally, use of homogenized effective properties is justified if the inherent length-scale ratio of the particles to the structure is below 1:50.

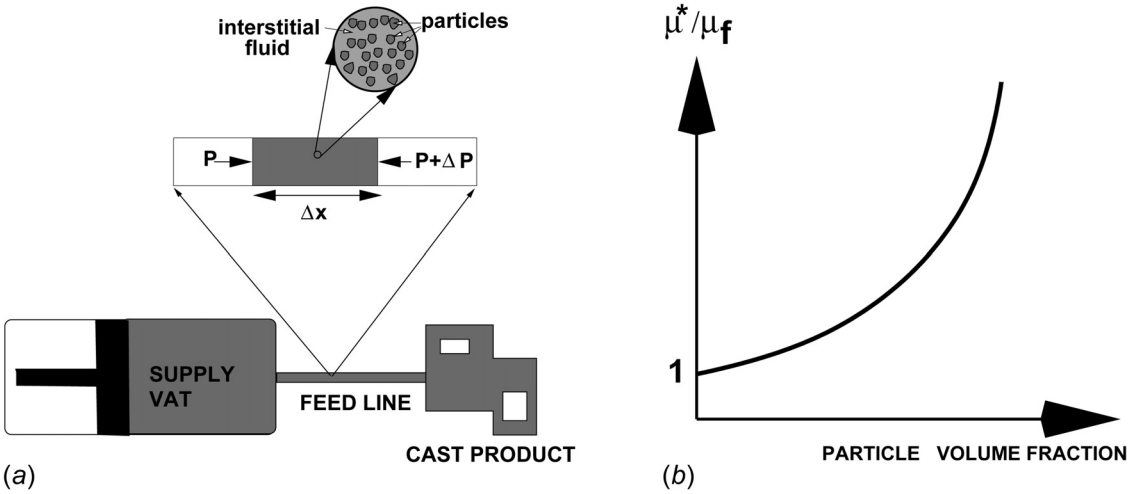

Fig. 1 (*a*) A particle-laden fluid in a channel and (*b*) the increase in the ratio of effective viscosity to baseline fluid viscosity (μ^*/μ_f) as a function of secondary particle volume fraction (v_p)

presence can dramatically increase the effective overall viscosity, thus requiring increased applied pressure to maintain nominal flow rates (Fig. 1). The primary objective of the first part of this analysis is to derive a relatively easy to use expression for the pressure gradient required to maintain a given flow rate in a channel, as a function of the volume fraction of secondary particles present in the fluid.

Accordingly, consider an idealized channel with a circular cross section of area $A = \pi R^2$, with a velocity profile given by a classical channel-flow of the form

$$v = v_{\max}\left(1 - \left(\frac{r}{R}\right)^q\right) \tag{1}$$

where $v_{\max}$ is the centerline velocity, and r is the radial coordinate from the centerline of the channel. For fully developed laminar flow, $q = 2$, while for increasing q one characterizes, phenomenologically, progressively turbulent flow ($q \geq 2$). The shear stress is given by

$$\tau = \mu^* \frac{\partial v}{\partial r} = -\frac{\mu^* v_{\max} q}{R}\left(\frac{r}{R}\right)^{q-1} \tag{2}$$

where μ^* is the effective viscosity of the particle-laden fluid. We assume that the overall flow rate is assumed constant, thus

$$Q = \int_A v dA = Q_o \tag{3}$$

One can show that

$$v_{\max} = \frac{Q_o(q+2)}{Aq} = \frac{Q_o(q+2)}{\pi R^2 q} \tag{4}$$

The stress at the wall becomes

$$\tau_w = -\tau(r = R) = \frac{\mu^* v_{\max} q}{R} = \frac{\mu^* Q_o(q+2)}{\pi R^3} \tag{5}$$

We have the following observations:

- Increasing μ^*, Q_o, or q increases the stress at the wall (τ_w),
- Increasing q leads to an increasingly more blunted flow profile, and
- Decreasing R increases the stress at the wall (τ_w).

Remark. In the remaining analysis, we will assume steady flow, the particles are not elongated and that they are well distributed within the base fluid.[3] Furthermore, we will adopt a generalization of the classical Poiseuille solution for fully developed flow in a pipe (assuming the velocity depends on some undetermined power q instead of the standard parabolic dependence for laminar single-phase flow).

3 Pressure Gradients

The previous expressions allow us to correlate the pressure applied to a volume of particle-laden to allow it to move as a constant flow rate. By performing a force balance, we have in the positive x-direction (assuming steady flow, no acceleration)

$$(-(P + \Delta P) + P)\pi R^2 - \tau_w 2\pi R \Delta x = 0 \tag{6}$$

where x is the coordinate along the length of the channel, and Δx is the differential length, leading to

$$-\Delta P = \mu^* \frac{Q_o(q+2)}{\pi^2 R^5} 2\pi R \Delta x = \frac{2\mu^* Q_o(q+2)\Delta x}{\pi R^4} \tag{7}$$

where we used the expression for $v_{\max}$ and where the effective viscosity is a function of the volume fraction of particles, $\mu^* = \mu^*(\nu_p)$. An explicit relation for $\mu^*(\nu_p)$ will be given shortly. Solving for the pressure gradient yields

$$-\frac{\Delta P}{\Delta x} = \underbrace{\frac{2\mu^*(q+2)}{\pi R^4}}_{C} Q_o \stackrel{\text{def}}{=} C Q_o \tag{8}$$

If we fix the flow rate Q_o, the multiplier C identifies the pressure gradient needed to achieve a flow rate Q_o. For a fixed value of q, the expression directly indicates that an increase in viscosity will require an increase in the pressure gradient. For small channels this can be a problem, as indicated by the R^4 term in the denominator. However, in general, q is a function of the Reynolds number. This case will be considered next.

4 Velocity Profile Characteristics

As the Reynolds number increases, the velocity profile will change from a quadratic ($q = 2$) to a more blunted profile ($q \gg 2$),

[3]In long channels, elongated particles can tend to align themselves in a particular direction that could also affect their viscosity. The assumptions made eliminate this possibility for the problems under consideration.

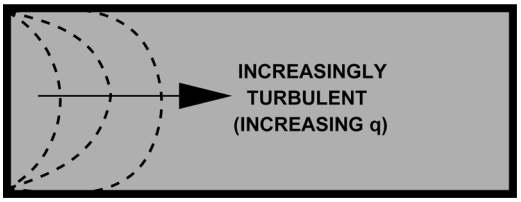

Fig. 2 Progressive blunting of the velocity profile with increasing Reynolds number

which represents, phenomenologically, turbulent (inertia-dominated) behavior (Fig. 2). The effect of a changing profile is described by representing q by a linear function of the centerline Reynolds' number ($\mathcal{R}_{ec}$)

$$q = q(\mathcal{R}_{ec}) = c_1\mathcal{R}_{ec} + c_2 \tag{9}$$

where $\mathcal{R}_{ec} = (\rho^* v_{max} 2R/\mu^*)$, and c_1 and c_2 are constants. Models of this type, linking the profile exponent (q) to the centerline Reynolds' number ($\mathcal{R}_{ec}$), are quite well-established, for example, see Hinze [16]. Usually, $0 \le c_1 \ll 1$ and $c_2 \approx 2$, and in the limit we have, for $c_1 = 0$ and $c_2 = 2$, laminar flow ($q = 2$). For the general case, combining Eq. (4) with Eq. (9) and the definition of the centerline Reynolds' number, we obtain a quadratic relationship for q

$$q^2 - (\gamma^* + c_2)q - 2\gamma^* = 0 \tag{10}$$

where $\gamma^* = (2c_1 Q_o \rho^*/\pi R\mu^*)$, where ρ^* is the effective density and μ^* is the effective viscosity. This quadratic relationship can be solved in closed form for q to yield[4]

$$q(\mathcal{R}_{ec}) = \frac{1}{2}\left((\gamma^* + c_2) \pm \sqrt{(\gamma^* + c_2)^2 + 8\gamma^*}\right) \tag{11}$$

The larger root is the physically correct choice (since the smaller root can become negative). We further observe that $q(\mathcal{R}_{ec})$ is a function of R^{-1} and decreasing R increases q, for fixed Q_o.

5 Models for Effective Properties of Particle-Laden Fluids

It is important to be able to characterize the effective properties of a particle-laden fluid as a function of the volume fraction of particles and the baseline (interstitial) fluid properties. The density of the particle-laden fluid is actually an "effective density," since it actually is a mixture of materials (particles and interstitial fluid). Effective properties are defined through volume averages. For example, the effective density of the mixture is

$$\rho^* \overset{\text{def}}{=} \langle \rho(\boldsymbol{x}) \rangle_V \overset{\text{def}}{=} \frac{1}{V}\int_V \rho(\boldsymbol{x})dV = \frac{1}{V}\left(\int_{V_f} \rho_f dV + \int_{V_p} \rho_p dV\right)$$
$$= \nu_f \rho_f + \nu_p \rho_p \tag{12}$$

where ν_f and ν_p are the volume fractions of the fluid and particles, respectively. The volume fractions have to sum to unity

$$\nu_f + \nu_p = 1 \Rightarrow \nu_f = 1 - \nu_p \tag{13}$$

Similar approaches can be used to calculate various types of properties, such as the effective viscosity (a transport property). However, to calculate them is a bit more complicated, since they require one to estimate the types of interaction between the constituents. There are a number of models which provide expressions for the effective viscosity of the fluid containing particles. For the purposes of this flow analysis, the particles are considered to be rigid, relative to the surrounding fluid. For example, in 1906, Einstein [17] developed an approximation which is quite simple, but only valid at extremely low volume fractions of particles (under one percent). It can be written as

$$\mu^* = \mu_f(1 + 2.5\nu_p) \tag{14}$$

where μ_f is the viscosity of the surrounding (incompressible) fluid, and the particles are assumed rigid. At even quite moderate to high volume fractions, this approximation is inaccurate. A better approximation, which is in fact a rigorous lower bound on the effective viscosity, can be derived from the well-known Hashin and Shtrikman [18–20] bounds (see Appendix A), and written as

$$\mu^* = \left(\mu_f\left(1 + 2.5\frac{\nu_p}{1 - \nu_p}\right)\right) \tag{15}$$

The expression above is the tightest known lower bound on the effective viscosity of a two-phase material comprising rigid particles in a surrounding incompressible fluid. The origin of the expression in Eq. (15) stems from bounds on effective responses for solid two-phase mixtures (see Appendix). This expression remains quite accurate up to about $\nu_p = 0.25$, which is sufficient for most applications and allows us to directly correlate the pressure gradient to the volume fraction of the particles. We refer the reader to Torquato [21] for more details.

6 Correlation of Pressure Gradient to Particle Volume Fraction

Using the effective properties, we have an expression for the velocity profile exponent

$$q(\mathcal{R}_{ec}(\mu^*, \rho^*), \gamma^*) = \frac{1}{2}\left((\gamma^* + c_2) \pm \sqrt{(\gamma^* + c_2)^2 + 8\gamma^*}\right) \tag{16}$$

Consequently, the pressure gradient's dependency on the volume fraction of particles can be written as

$$-\frac{\Delta P}{\Delta x} = \frac{2\left(\mu_f\left(1 + 2.5\frac{\nu_p}{1-\nu_p}\right)\right)(q(\mathcal{R}_{ec}(\mu^*, \rho^*), \gamma^*) + 2)}{\pi R^4} Q_o \overset{\text{def}}{=} C^* Q_o \tag{17}$$

where $C^* = C^*(Q_o)$. For a fixed flow rate, Q_o, increasing the volume fraction of particles (ν_p) requires a corresponding increase in the pressure differential. Explicitly, the Reynolds number is

$$R_e = \frac{v_{max} D\rho^*}{\mu^*} = \frac{2Q_o(q+2)}{\pi R q}\frac{((1-\nu_p)\rho_f + \nu_p\rho_p)}{\mu_f\left(1 + 2.5\frac{\nu_p}{1-\nu_p}\right)} \tag{18}$$

7 Trends

To illustrate the trends, we varied Q_o from 10^{-3} m^3/s to 10^{-2} m^3/s and utilized the expression in Eq. (17). We plotted the pressure gradient and Reynolds number as a function of the volumetric flow rate (Q_o) in Fig. 3 for various values of ν_p, with the following parameters used:[5]

- Viscosity: $\mu_f = 0.01$ Pa s,
- Fluid density: $\rho_f = 2000$ kg/m^3,

[4] In the special case of laminar flow ($c_1 = 0$ and $c_2 = 2$), there are two roots to Eq. (11), $q = 2$ and $q = 0$.

[5] For reference, the viscosity of water is $\mu_f = 0.001$ Pa s and for honey is $\mu_f = 1$ Pa s.

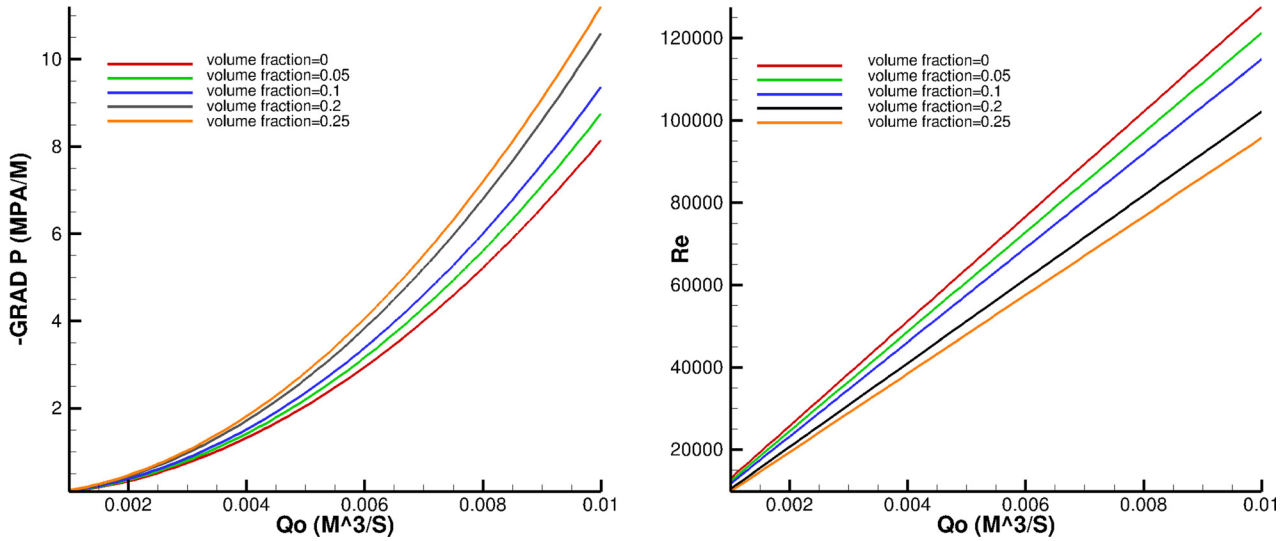

Fig. 3 Trends—Left: the pressure gradient needed ($-(\Delta P/\Delta x)$) as a function of the desired volumetric flow rate (Q_o) for various volume fractions of v_p. Right: the resulting Reynolds number as a function of the volumetric flow rate (Q_o).

- Particle density: $\rho_p = 5000\,\text{kg/m}^3$,
- Channel radius: $R = 0.01$ m, and
- Profile constants: $c_1 = 0.01$ and $c_2 = 2$.

Generally, the trends are that a steady increase in the pressure gradient (approximately 40% more) is needed to maintain a fixed Q_o, for increasing the volume fraction of particles. Due to the increase in the particle volume fraction, the viscosity increases, thus decreasing the Reynolds number. High Reynolds numbers, and consequential turbulence, can lead to aspiration (air entrainment), spurious internal reactions, dewetting, etc., which can lead to voids. The point of this example was not to illustrate an all encompassing parameter set, but simply to show the explicit dependency of the pressure gradient and Reynolds number on the presence of secondary particles. Other parameter sets can be easily simulated.

8 Summary

The presence of particle-laden fluids is widespread. Because the presence of particles increases the overall viscosity of the fluid, the pressure gradients needed to pump such fluids through channels at a nominal flow rate can increase dramatically. The present analysis and model can provide a useful guide to designing systems that pump particle-laden flows, with the purpose to be able to cast materials. This paper derived the pressure gradient needed to maintain a given flow rate, as a function volume fraction of particles present in the fluid. The expression explicitly correlates the dependency of the pressure gradient to the particle volume fraction and is hopefully easy to use by researchers in the field. Furthermore, the developed expressions also provide estimates on the Reynolds numbers that arise for given flow rates. The tracking of the Reynolds number is important, since turbulence can lead to improper casting due to the resulting voids. For example, one can estimate the reduction of the material quality as a function of the porous material by assuming that it comprises an isotropic elastic matrix, with a bulk modulus κ_m and shear modulus μ_m, while the porous void space is modeled by an elastic material with very low bulk and shear moduli $\kappa_v = \delta\kappa_m$, $\mu_v = \delta\mu_m$, with $0 \le \delta \ll 1$. The exact case of voids corresponds to $\delta \to 0$. To estimate the properties of the material with voids, we employ the Hashin–Shtrikman bounds (see Appendix), assign the following (the harder material is the matrix and the softer is the voids): $\kappa_v = \kappa_1$, $\mu_v = \mu_1$ and $\kappa_m = \kappa_2$, $\mu_m = \mu_2$, $\nu_v = \nu_1$ and $\nu_m = \nu_2$, and force $\mu_v \to 0$ and $\kappa_v \to 0$ to obtain

$$0 \le \kappa^{*,\text{voids}} \le \kappa_m(1 - \nu_v G(\nu_v)) \tag{19}$$

where

$$G(\nu_v) = \frac{3\kappa_m + 4\mu_m}{3\nu_v\kappa_m + 4\mu_m} \tag{20}$$

and

$$0 \le \mu^{*,\text{voids}} \le \mu_m(1 - \nu_v C(\nu_v)) \tag{21}$$

where

$$C(\nu_v) = \frac{5(3\kappa_m + 4\mu_m)}{\kappa_m(9 + 6\nu_v) + \mu_m(8 + 12\nu_v)} \tag{22}$$

One can then assign the effective properties of the void-free part of the particle-laden mixture to the matrix material, $\kappa^{*,\text{no-voids}} = \kappa_m$ and $\mu^{*,\text{no-voids}} = \mu_m$, leading to

$$0 \le \kappa^{*,\text{voids}} \le \kappa^{*,\text{no-voids}}(1 - \nu_v G(\nu_v)) \tag{23}$$

and

$$0 \le \mu^{*,\text{voids}} \le \mu^{*,\text{no-voids}}(1 - \nu_v C(\nu_v)) \tag{24}$$

It is important to note that

- As $\nu_v \to 1, \nu_v G(\nu_v) \to 1$ and $\nu_v C(\nu_v) \to 1$, thus $\mu^{*,\text{voids}} \to 0$ and
- As $\nu_v \to 0, \nu_v G(\nu_v) \to 0$ and $\nu_v C(\nu_v) \to 0$, thus $\mu^{*,\text{voids}} \to \mu^{*,\text{no-voids}}$.

These expressions show the resulting effective property loss as a function of the voids. Further expressions on the reduction of material performance are provided in Appendix B. We remark that in some applications, such as biomedical devices, controlled porosity with prespecified pore shapes, sizes, and distributions is sought after using, for example, porogen templating processes. We refer the reader to Hong et al. [22] for a detailed overview of the state of the art of porogen patterning. Other emerging, cutting-edge, approaches for controlled generation of desired porosity involve laser processing (Kongsuwan et al. [23]). This is particularly useful for precisely functionalized layered substrates.

In summary, the present analysis and model can provide a useful guide to designing and interpreting experiments. However, while the model can provide qualitative information, extensions are almost certainly going to require complex spatiotemporal discretization resolving multiparticle particle–fluid interaction. Such particle/fluid systems are strongly coupled, due to the drag forces induced by the fluid onto the particles and vice versa. For example, in Zohdi [13,14], a flexible and robust solution strategy was developed to resolve coupled systems comprising large groups of flowing particles embedded within a continuous flowing fluid. The focus of that work was to develop adaptive time-stepping schemes which properly resolve the coupling, via a staggered recursive time-stepping process. The approach can be used in conjunction with computational fluid mechanics codes based on finite difference, finite element, finite volume, or discrete element discretization, for example, such as those developed in Onate et al. [2,3], Rojek et al. [4], Carbonell et al. [5], Labra and Onate [6], Leonardi et al. [7], Cante et al. [8], Rojek [9], Onate et al. [10], Bolintineanu et al. [11], Avci and Wriggers [12], and Zohdi [24–26]. Finally, we mention that oftentimes the detrimental growth of channel walls (thus clogging feed lines) starts with the adhesion of particles to the surfaces. This is a complex process, which is likely to involve low fluid-induced shear stress (allowing particles stick to the walls, Zohdi [27,28] and Zohdi et al. [29]) and strongly coupled diffusive, chemical effects, and thermal effects. The application of such computational procedures to the problems considered in this paper is under current investigation by the author.

Appendix A: Effective Property Bounds

The literature on methods to estimate the overall macroscopic properties of heterogeneous materials dates back at least to Maxwell [30,31] and Rayleigh [32], with a notable contribution being the Hashin–Shtrikman bounds [18–20]. The Hashin–Shtrikman bounds are the tightest possible bounds on isotropic effective responses, generated from isotropic microstructures, where the volumetric data and phase contrasts of the constituents are the only data known. For linearized elasticity applications, for isotropic materials with isotropic effective (mechanical) responses, the Hashin–Shtrikman bounds (for a two-phase material) are as follows:

$$\kappa^{*,-} \stackrel{\text{def}}{=} \kappa_1 + \frac{\nu_2}{\frac{1}{\kappa_2-\kappa_1}+\frac{3(1-\nu_2)}{3\kappa_1+4G_1}} \leq \kappa^* \leq \kappa_2 + \frac{1-\nu_2}{\frac{1}{\kappa_1-\kappa_2}+\frac{3\nu_2}{3\kappa_2+4G_2}} \stackrel{\text{def}}{=} \kappa^{*,+} \tag{A1}$$

and for the shear modulus

$$G^{*,-} \stackrel{\text{def}}{=} G_1 + \frac{\nu_2}{\frac{1}{G_2-G_1}+\frac{6(1-\nu_2)(\kappa_1+2G_1)}{5G_1(3\kappa_1+4G_1)}} \leq G^* \leq G_2 + \frac{(1-\nu_2)}{\frac{1}{G_1-G_2}+\frac{6\nu_2(\kappa_2+2G_2)}{5G_2(3\kappa_2+4G_2)}} \stackrel{\text{def}}{=} G^{*,+} \tag{A2}$$

where κ_2 and κ_1 are the bulk moduli, and G_2 and G_1 are the shear moduli of the respective phases ($\kappa_2 \geq \kappa_1$ and $G_2 \geq G_1$), and where ν_2 is the second phase volume fraction. Such bounds are the tightest possible on isotropic effective responses, with isotropic two-phase microstructures, where only the volume fractions and phase contrasts of the constituents are known. Note that no geometric or statistical information is required for the bounds. For an authoritative review of (a) the general theory of random heterogeneous media see, for example, Torquato [21], (b) for more mathematical homogenization aspects, see Jikov et al. [33], and (c) for solid-mechanics inclined accounts of the subject see, for example, Hashin [20], Mura [34], or Markov [35]. We note that numerical methods have become the dominant tool for determining effective properties. In particular, finite element-based methods are extremely popular, and we refer the reader to Ghosh [36], Ghosh and Dimiduk [37], and Zohdi and Wriggers [15].

Finally, to derive Eq. (15), one can take the limit of the particle phase becoming rigid, i.e., the bulk and shear moduli tending toward infinity, $\kappa_p \to \infty$ and $G_p \to \infty$, signifying that the particles are much stiffer than the interstitial fluid, while simultaneously specifying that the interstitial fluid is incompressible, i.e., $\kappa_f/G_f \to \infty$ with G_f being finite. This yields

$$G^* = G_f\left(1 + 2.5\frac{\nu_p}{1-\nu_p}\right) \tag{A3}$$

One can then assign μ_f, the value of G_f to obtain Eq. (15). See, for example, Abedian and Kachanov [38] and Sevostianov and Kachanov [39] for more details.

Appendix B: Reduction in Failure Strength Due to Voids

The failure of most structural materials is associated with reaching a critical deviatoric stress. In order to determine the reduction in failure strength due to voids, we denote the macroscopic effective elastic shear modulus as $\mu^{*,\text{voids}}$ and the deviatoric stress at yield as $\boldsymbol{\Sigma}^{*,\text{voids},\prime}$. To start the analysis, we consider the dense material to have met the failure stress ($\boldsymbol{\Sigma}'_m$), thus yielding an expression for the overall failure stress ($\boldsymbol{\Sigma}^{*,\text{voids},\prime}$)

$$\begin{aligned}\langle \boldsymbol{\sigma}' \rangle_\Omega &= \nu_v \langle \boldsymbol{\sigma}' \rangle_{\Omega_v} + \nu_m \langle \boldsymbol{\sigma}' \rangle_{\Omega_m} = \nu_m \langle \boldsymbol{\sigma}' \rangle_{\Omega_m} \\ &= (1-\nu_v)\langle \boldsymbol{\sigma}' \rangle_{\Omega_m} = (1-\nu_v)\boldsymbol{\Sigma}'_m = \boldsymbol{\Sigma}^{*,\text{voids},\prime}\end{aligned} \tag{B1}$$

where $\boldsymbol{\Sigma}'_m$ is the stress at which the dense material fails. The effective shear modulus needed to determine $\left(\boldsymbol{\Sigma}^{*,\text{voids},\prime}/2\mu^{*,\text{voids}}\right)$ can be estimated as in the main body of the text. Thus, for the small overall strains at which macroscopic failure occurs

$$\begin{aligned}2\mu^{*,\text{voids}}\langle \boldsymbol{\epsilon}'_v \rangle_\Omega &= 2\mu^{*,\text{voids}}\boldsymbol{Y}'^{,*,\text{voids}} \approx 2\mu_m(1-C(\nu_v))\boldsymbol{Y}'^{,*,\text{voids}} \\ &= \langle \boldsymbol{\sigma}' \rangle_\Omega \approx \boldsymbol{\Sigma}'_m(1-\nu_v)\end{aligned} \tag{B2}$$

and thus

$$\boldsymbol{Y}'^{,\text{voids},*} = \left(\frac{\boldsymbol{\Sigma}'_m}{2\mu_m}\right)\underbrace{\left(\frac{1-\nu_v}{1-\nu_v C(\nu_v)}\right)}_{\stackrel{\text{def}}{=}\Phi(\nu_v)} \tag{B3}$$

where $\boldsymbol{Y}'^{,\text{voids},*}$ is the macroscopic small strain deviator at initial failure. Thus, we have

$$\boldsymbol{Y}'^{,\text{voids},*} \approx \frac{\boldsymbol{\Sigma}^{*,\text{voids},\prime}}{2\mu^{*,\text{voids}}} \approx \left(\frac{\boldsymbol{\Sigma}'_m}{2\mu_m}\right)\Phi(\nu_v) \tag{B4}$$

where the function $\Phi(\nu_v)$ is a *slowly* increasing function of ν_v. *It is noted that since an upper bound was used in the construction of $C(\nu_v)$, and due to the functional dependence of Φ on $C(\nu_v)$, Φ is an overestimation of the increase in the overall failure strain.* One can then assign the effective properties of the slurry and binder to the matrix material, $\mu^{*,\text{no-voids}} = \mu_m$, $\boldsymbol{\Sigma}'_m = \boldsymbol{\Sigma}'^{,\text{no-voids},*}$, and $\boldsymbol{Y}'_m = \boldsymbol{Y}'^{,\text{no-voids},*}$. Thus, the change in the yield stress is

$$\boldsymbol{\Sigma}'^{,\text{voids},*} = \boldsymbol{\Sigma}'^{,\text{no-voids},*}(1-\nu_{\text{v}}) \tag{B5}$$

and the change in yield strain is

$$\boldsymbol{Y}'^{,\text{voids},*} \approx \left(\frac{\boldsymbol{\Sigma}'^{,\text{no-voids},*}}{2\mu^{*,\text{no-voids}}}\right)\Phi(\nu_{\text{v}}) = \boldsymbol{Y}'^{,\text{no-voids},*}\Phi(\nu_{\text{v}}) \tag{B6}$$

References

[1] Wei, C., and Dong, J., 2014, "Development and Modeling of Melt Electrohydrodynamic-Jet Printing of Phase-Change Inks for High-Resolution Additive Manufacturing," ASME J. Manuf. Sci. Eng., **136**(6), p. 061010.

[2] Onate, E., Idelsohn, S. R., Celigueta, M. A., and Rossi, R., 2008, "Advances in the Particle Finite Element Method for the Analysis of Fluid-Multibody Interaction and Bed Erosion in Free Surface Flows," Comput. Methods Appl. Mech. Eng., **197**(19–20), pp. 1777–1800.

[3] Onate, E., Celigueta, M. A., Idelsohn, S. R., Salazar, F., and Suárez, B., 2011, "Possibilities of the Particle Finite Element Method for Fluid-Soil-Structure Interaction Problems," Comput. Mech., **48**(3), pp. 307–318.

[4] Rojek, J., Labra, C., Su, O., and Onate, E., 2012, "Comparative Study of Different Discrete Element Models and Evaluation of Equivalent Micromechanical Parameters," Int. J. Solids Struct., **49**(13), pp. 1497–1517.

[5] Carbonell, J. M., Onate, E., and Suarez, B., 2010, "Modeling of Ground Excavation With the Particle Finite Element Method," J. Eng. Mech., ASCE, **136**(4), pp. 455–463.

[6] Labra, C., and Onate, E., 2009, "High-Density Sphere Packing for Discrete Element Method Simulations," Commun. Numer. Methods Eng., **25**(7), pp. 837–849.

[7] Leonardi, A., Wittel, F. K., Mendoza, M., and Herrmann, H. J., 2014, "Coupled DEM-LBM Method for the Free-Surface Simulation of Heterogeneous Suspensions," Comput. Part. Mech., **1**(1), pp. 3–13.

[8] Cante, J., Davalos, C., Hernandez, J. A., Oliver, J., Jonsen, P., Gustafsson, G., and Haggblad, H. A., 2014, "PFEM-Based Modeling of Industrial Granular Flows," Comput. Part. Mech., **1**(1), pp. 47–70.

[9] Rojek, J., 2014, "Discrete Element Thermomechanical Modeling of Rock Cutting With Valuation of Tool Wear," Comput. Part. Mech., **1**(1), pp. 71–84.

[10] Onate, E., Celigueta, M. A., Latorre, S., Casas, G., Rossi, R., and Rojek, J., 2014, "Lagrangian Analysis of Multiscale Particulate Flows With the Particle Finite Element Method," Comput. Part. Mech., **1**(1), pp. 85–102.

[11] Bolintineanu, D. S., Grest, G. S., Lechman, J. B., Pierce, F., Plimpton, S J., and Schunk, P. R., 2014, "Particle Dynamics Modeling Methods for Colloid Suspensions," Comput. Part. Mech., **1**(3), pp. 321–356.

[12] Avci, B., and Wriggers, P., 2012, "A DEM-FEM Coupling Approach for the Direct Numerical Simulation of 3D particulate Flows," ASME J. Appl. Mech., **79**(1), p. 010901.

[13] Zohdi, T. I., 2007, "Computation of Strongly Coupled Multifield Interaction in Particle-Fluid Systems," Comput. Methods Appl. Mech. Eng., **196**(37), pp. 3927–3950.

[14] Zohdi, T. I., 2014, "Embedded Electromagnetically Sensitive Particle Motion in Functionalized Fluids," Comput. Part. Mech., **1**(1), pp. 27–45.

[15] Zohdi, T. I., and Wriggers, P., 2008, *Introduction to Computational Micromechanics*, Springer, Berlin.

[16] Hinze, J. O., 1975, *Turbulence*, McGraw-Hill, New York.

[17] Einstein, A., 1906, "A New Determination of Molecular Dimensions," Ann. Phys., **19**(4), pp. 289–306.

[18] Hashin, Z., and Shtrikman, S., 1962, "On Some Variational Principles in Anisotropic and Nonhomogeneous Elasticity," J. Mech. Phys. Solids, **10**(4), pp. 335–342.

[19] Hashin, Z., and Shtrikman, S., 1963, "A Variational Approach to the Theory of the Elastic Behaviour of Multiphase Materials," J. Mech. Phys. Solids, **11**(2), pp. 127–140.

[20] Hashin, Z., 1983, "Analysis of Composite Materials: A Survey," ASME J. Appl. Mech., **50**(3), pp. 481–505.

[21] Torquato, S., 2002, *Random Heterogeneous Materials: Microstructure and Macroscopic Properties*, Springer, New York.

[22] Hong, Y., Zhou, J. G., and Yao, D., 2014, "Porogen Templating Processes: An Overview," ASME J. Manuf. Sci. Eng., **136**(3), p. 031013.

[23] Kongsuwan, P., Brandal, G., and Yao, Y. L., 2015, "Laser Induced Porosity and Crystallinity Modification of a Bioactive Glass Coating on Titanium Substrates," ASME J. Manuf. Sci. Eng., **137**(3), p. 031004.

[24] Zohdi, T. I., 2013, "Numerical Simulation of Charged Particulate Cluster-Droplet Impact on Electrified Surfaces," J. Comput. Phys., **233**, pp. 509–526.

[25] Zohdi, T. I., 2012, *Dynamics of Charged Particulate Systems. Modeling, Theory and Computation*, Springer, Heidelberg.

[26] Zohdi, T. I., 2004, "A Computational Framework for Agglomeration in Thermo-Chemically Reacting Granular Flows," Proc. R. Soc., **460**(2052), pp. 3421–3445.

[27] Zohdi, T. I., 2005, "A Simple Model for Shear Stress Mediated Lumen Reduction in Blood Vessels," Biomech. Model. Mechanobiol., **4**(1), pp. 57–61.

[28] Zohdi, T. I., 2014, "Mechanically-Driven Accumulation of Microscale Material at Coupled Solid-Fluid Interfaces in Biological Channels," Proc. R. Soc. Interface, **11**(91), p. 20130922.

[29] Zohdi, T. I., Holzapfel, G. A., and Berger, S. A., 2004, "A Phenomenological Model for Atherosclerotic Plaque Growth and Rupture," J. Theor. Biol., **227**(3), pp. 437–443.

[30] Maxwell, J. C., 1867, "On the Dynamical Theory of Gases," Philos. Trans. Soc. London, **157**, pp. 49–88.

[31] Maxwell, J. C., 1873, *A Treatise on Electricity and Magnetism*, 3rd ed., Clarendon Press, Oxford, UK.

[32] Rayleigh, J. W., 1892, "On the Influence of Obstacles Arranged in Rectangular Order Upon Properties of a Medium," Philos. Mag. **32**, pp. 481–491.

[33] Jikov, V. V., Kozlov, S. M., and Olenik, O. A., 1994, *Homogenization of Differential Operators and Integral Functionals*, Springer, Berlin.

[34] Mura, T., 1993, *Micromechanics of Defects in Solids*, 2nd ed., Kluwer Academic Publishers, Springer-Verlag, Berlin.

[35] Markov, K. Z., 2000, "Elementary Micromechanics of Heterogeneous Media," *Heterogeneous Media: Micromechanics Modeling Methods and Simulations*, K. Z. Markov, and L. Preziozi, eds., Birkhauser, Boston, MA, pp. 1–162.

[36] Ghosh, S., 2011, *Micromechanical Analysis and Multi-Scale Modeling Using the Voronoi Cell Finite Element Method*, CRC Press/Taylor & Francis, Boca Raton, FL.

[37] Ghosh, S., and Dimiduk, D., 2011, *Computational Methods for Microstructure-Property Relations*, Springer, New York.

[38] Abedian, B., and Kachanov, M., 2010, "On the Effective Viscosity of Suspensions," Int. J. Eng. Sci., **48**(11), pp. 962–965.

[39] Sevostianov, I., and Kachanov, M., 2012, "Effective Properties of Heterogeneous Materials: Proper Application of the Non-Interaction and the "Dilute Limit" Approximations," Int. J. Eng. Sci., **58**, pp. 124–128.